OXFORD

Human Molecular Genetics, 2017, Vol. 26, No. 10 1890–1899

doi: 10.1093/hmg/ddx097
Advance Access Publication Date: 13 March 2017
Original Article

ORIGINAL ARTICLE

Downregulation of pathways implicated in liver inflammation and tumorigenesis of glycogen storage disease type Ia mice receiving gene therapy

Goo-Young Kim[1], Joon Hyun Kwon[1], Jun-Ho Cho[1], Lisa Zhang[1], Brian C. Mansfield[1,2] and Janice Y. Chou[1,*]

[1]Section on Cellular Differentiation, Eunice Kennedy Shriver National Institute of Child Health and Human Development, National Institutes of Health, Bethesda, MD 20892, USA and [2]Foundation Fighting Blindness, Columbia, MD 21046, USA

*To whom correspondence should be addressed. Tel: 301 4961094; Fax: 301 4026035; Email: chouja@mail.nih.gov

Abstract

Glycogen storage disease type Ia (GSD-Ia) is characterized by impaired glucose homeostasis and long-term risks of hepatocellular adenoma (HCA) and carcinoma (HCC). We have shown that the non-tumor-bearing (NT), recombinant adeno-associated virus (rAAV) vector-treated GSD-Ia mice (AAV-NT mice) expressing a wide range (0.9–63%) of normal hepatic glucose-6-phosphatase-α activity maintain glucose homeostasis and display physiologic features mimicking animals living under calorie restriction (CR). We now show that in AAV-NT mice, the signaling pathways of the CR mediators, AMP-activated protein kinase (AMPK) and sirtuin-1 are activated. AMPK/sirtuin-1 inhibit the activity of STAT3 (signal transducer and activator of transcription 3) and NFκB (nuclear factor κB), the pro-inflammatory and cancer-promoting transcription factors. Sirtuin-1 also inhibits cancer metastasis via increasing the expression of E-cadherin, a tumor suppressor, and decreasing the expression of mesenchymal markers. Consistently, in AAV-NT mice, hepatic levels of active STAT3 and NFκB-p65 were reduced as were expression of mesenchymal markers, STAT3 targets, NFκB targets and β-catenin targets, all of which were consistent with the promotion of tumorigenesis. AAV-NT mice also expressed increased levels of E-cadherin and fibroblast growth factor 21 (FGF21), targets of sirtuin-1, and β-klotho, which can acts as a tumor suppressor. Importantly, treating AAV-NT mice with a sirtuin-1 inhibitor markedly reversed many of the observed anti-inflammatory/anti-tumorigenic signaling pathways. In summary, activation of hepatic AMPK/sirtuin-1 and FGF21/β-klotho signaling pathways combined with down-regulation of STAT3/NFκB-mediated inflammatory and tumorigenic signaling pathways can explain the absence of hepatic tumors in AAV-NT mice.

Introduction

Hepatocellular adenoma (HCA) and hepatocellular carcinoma (HCC) are long term risks for patients with the metabolic disease glycogen storage disease type Ia (GSD-Ia, MIM232200). The early hallmark of GSD-Ia is impaired blood glucose homeostasis, caused by a deficiency in the enzyme glucose-6-phosphatase-α (G6Pase-α or G6PC) (1,2). Untreated, GSD-Ia is juvenile lethal. Dietary therapies (3,4) have enabled GSD-Ia patients to attain near normal growth and pubertal development. However, no current therapy is able to address the long-term complication of HCA that develops in 75% of GSD-I patients over 25 years-old (1,2). In addition to the associated life threatening complications of intratumor haemorrhage of HCA, 10% of HCA cases undergo malignant transformation to hepatocellular carcinoma (HCC) (1,2,5). In GSD patients classified to date, 52% of HCA are inflammatory HCA, 28% β-catenin mutated HCA and 20% unclassified HCA (6,7).

Received: February 1, 2017. **Revised:** March 6, 2017. **Accepted:** March 8, 2017

We have evaluated the efficacy of gene therapy mediated by recombinant adeno-associated virus (rAAV) pseudotype 2/8 vectors expressing the wild-type human G6Pase-α (rAAV-G6PC) and a codon optimized (co) human G6Pase-α (rAAV-co-G6PC), both directed by the human *G6PC* promoter/enhancer (8–11). Previously, we showed that systemic administration of rAAV-G6PC (8–11) or rAAV-co-G6PC (10) delivers the G6Pase-α transgene to the liver of *G6pc*-/- mice and provides a sustained correction of metabolic abnormalities for up to 90 weeks (8–11). Titrating the viral dose to vary the level of G6Pase-α expression, we have examined tumor development in 55 rAAV-treated *G6pc*-/- mice expressing 0.9–63% of normal hepatic G6Pase-α activity (8–11). Thirty-eight of the treated mice expressed 3–63% of normal hepatic G6Pase-α activity (AAV/3–63% mice) and none developed HCA/HCC (8–10). While 3 of the 17 treated mice expressed 0.9–2.4% of normal hepatic G6Pase-α activity (AAV/0.9–2.4% mice) developed HCA/HCC, 14 of these were not tumor-bearing (NT) (AAV/0.9–2.4%-NT mice) (10,11). In this study, we delineate the pathways that may explain why AAV/3–63% and AAV/0.9–2.4%-NT mice do not develop HCA/HCC.

While GSD-Ia is a disease of the liver, kidney and intestine, the primary disease target is the liver. The rAAV8-mediated G6Pase-α transgene expression primarily targets the liver with little transgene expression observed in the kidney and intestine (12). In the absence of endogenous glucose production from the kidney and intestine, the AAV/3–63% mice display physiologic features mimicking animals living under calorie restriction (CR) and are protected against age-related obesity and insulin resistance (9,10). We have previously shown that activation of hepatic AMP-activated protein kinase (AMPK)/sirtuin-1 (SIRT1) signaling is one pathway responsible for the improved metabolic phenotype of the AAV/3–63% mice (9). We now show that hepatic AMPK/SIRT1 signaling is also activated in the AAV/0.9–2.4%-NT mice.

AMPK and SIRT1 are two modulators of CR that are involved in regulation of energy metabolism (13). AMPK is a master regulator of energy homeostasis and is activated by CR (14,15). AMPK inhibits interleukin-6 (IL-6)-mediated phosphorylation of signal transducer and activator of transcription 3 (STAT3) (16), a cancer-promoting transcription factor that is constitutively activated in inflammatory HCA in GSD-Ia (7). Phosphorylation of STAT3 at Y705 triggers STAT3 homodimerization and nuclear translocation that lead to transcriptional activation of target genes and stimulate a cancer-promoting inflammatory response (16,17). SIRT1 is a NAD^+-dependent deacetylase that can be activated at the transcriptional levels or in response to an increase in cellular NAD^+ levels (18). SIRT1 (18,19) deacetylates residue K310 on the p65 subunit of nuclear factor κB (NFκB) and represses the activity of NFκB, a transcription factor that regulates inflammation and promotes inflammation-associated cancer (20–22). Importantly, the signaling by STAT3 and NFκB is highly interconnected (17). Together they regulate many genes involved in tumor proliferation, survival, and invasion. Studies have shown that liver inflammation promotes HCC development, and STAT3 and NFκB play important roles in HCC development and progression (22).

SIRT1 is also a negative regulator of tumor metastasis that increases the expression of E-cadherin and decreases the expression of the mesenchymal markers, N-cadherin and vimentin (23). E-Cadherin in turn is a cell-cell adhesion molecule that regulates epithelial-mesenchymal transition (EMT) (24). The decrease in E-cadherin expression leads to a loss of cell-cell adhesion and the initiation of metastasis. Moreover the cytoplasmic domain of E-cadherin interacts with catenins to form a cadherin-catenin complex that modulates various signaling pathways in epithelial cells (24), such as the Wnt/β-catenin pathway implicated in the β-catenin mutated HCA (6,7). E-Cadherin also acts as a tumor suppressor by sequestering β-catenin at sites of cell-cell contact and inhibiting Wnt/β-catenin signaling (24).

Caloric restriction also increases hepatic expression of fibroblast growth factor 21 (FGF21) and β-klotho (25) which is a co-receptor of FGF21 (26). As a major regulator of energy metabolism and a downstream target activated by SIRT1 (27), FGF21 stimulates energy expenditure, fat utilization and lipid excretion (26). β-Klotho is a tumor suppressor that inhibits the proliferation of hepatoma cells (28). A recent study showed that FGF21 can prevent diethylnitrosamine-induced hepatocarcinogenesis by increasing the expression of β-klotho (29). So AMPK, SIRT1, FGF21 and β-klotho are of particular interest in elucidating the mechanisms that suppress HCA/HCC formation in AAV/3–63% and AAV/0.9–2.4%-NT mice.

In this study, we provide evidence that the underlying mechanisms responsible for the absence of HCA/HCC in AAV/3-63% and AAV/0.9–2.4%-NT mice correlate with activation of hepatic AMPK/SIRT1 and FGF21/β-klotho signaling pathways and down-regulation of hepatic STAT3/NFκB-mediated inflammatory and tumorigenic signaling pathways. Our findings lend insight into the mechanisms underlying the absence of HCA/HCC observed in the treated GSD-Ia mice, and provide guidance to the design of gene therapy in human may have the potential to reduce the long term risks of HCA/HCC.

Results

Activation of hepatic AMPK/SIRT1 signaling

We have shown that AAV/3–63% mice with hepatic expression of 3–63% (5–108 units) of normal hepatic G6Pase-α activity (171.8 ± 7.1 units) maintain blood glucose homeostasis, lack HCA/HCC, and do not develop the typical age-related obesity and insulin resistance of their age matched wild-type counterparts (9). We have further shown that that activation of hepatic AMPK/SIRT1 signaling is one pathway responsible for the improved metabolic phenotype of these mice (9). More recently, we showed that non-tumor-bearing AAV/0.9–2.4%-NT mice also maintain glucose homeostasis and are protected against age-related obesity and insulin resistance (10). We therefore examined whether AMPK/SIRT1 signaling is activated in these mice. Compared to wild-type mice, hepatic protein levels of AMPK and the active p-AMPK-T172 were elevated in both AAV/3–63% and AAV/0.9–2.4%-NT mice (Fig. 1A). SIRT1 is a NAD^+-dependent deacetylase that can be activated in response to an increase in cellular NAD^+ levels (18). While hepatic protein levels of SIRT1 were unchanged between wild-type and the rAAV-treated *G6pc*-/- mice (Fig. 1A), hepatic NAD^+ concentrations were significantly elevated in all rAAV treated mice, compared to the controls (Fig. 1B), consistent with SIRT1 activation. In summary, the phenotypes of AAV/3–63% and AAV/0.9–2.4%-NT mice were indistinguishable and collectively named by the non-tumor phenotype as the AAV-NT mice.

Down-regulation of STAT3 and NFκB signaling pathways in AAV-NT mice

The most prevalent subtype of HCA observed in GSD is inflammatory HCA, which is characterized by a constitutive activation of STAT3 (7). Studies have shown that AMPK suppresses

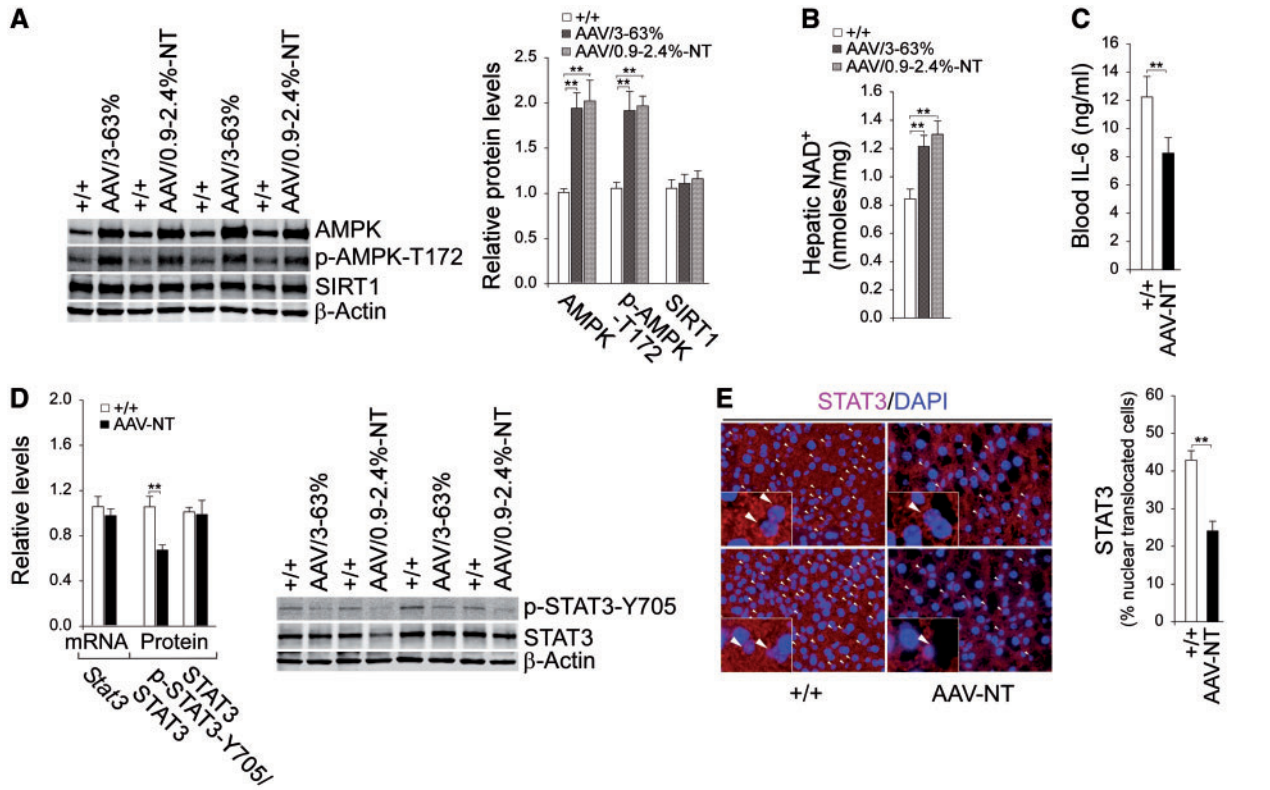

Figure 1. Analysis of hepatic AMPK, SIRT1 and STAT3 signaling in 66–88 week-old wild-type and rAAV-treated *G6pc*-/- mice. For quantitative RT-PCR, the data were analyzed for wild-type (+/+, $n = 13$) and AAV-NT ($n = 22$) mice. **(A)** Western-blot analysis of AMPK, p-AMPK-T172, SIRT1 and β-actin with quantification of protein levels by densitometry in wild-type ($n = 8$), AAV/3–63% (n = 4) and AAV/0.9–2.4%-NT ($n = 4$) mice. **(B)** Hepatic NAD^+ levels in wild-type ($n = 13$), AAV/3–63% ($N = 8$), and AAV/0.9–2.4%-NT ($n = 8$) mice. **(C)** Blood IL-6 levels in wild-type ($n = 13$) and AAV-NT ($n = 16$) mice. **(D)** Quantification of *Stat3* mRNA by real-time RT-PCR; Western blot analysis of p-STAT3-Y705, STAT3 and β-actin with quantification of protein levels by densitometry from 4 pairs of wild-type/AAV-NT mice. The AAV-NT analyzed included AAV/3–63% ($n = 2$) and AAV/0.9–2.4%-NT ($n = 2$) mice. **(E)** Immunofluorescence analysis of hepatic STAT3 nuclear localization and quantification of nuclear STAT3-translocated cells. Representative plates shown are analyzed for wild-type mice ($n = 6$) and AAV-NT ($n = 5$) mice. Scale bar: 25 μm. Arrows denote STAT3-positive nuclei. Data represent the mean ± SEM; $^{**}P < 0.005$.

inflammation by inhibiting IL-6-mediated phosphorylation and activation of STAT3 signaling (16). The phosphorylation of STAT3 at Y705 triggers nuclear translocation and activation of STAT3 regulated genes (16,17). Compared to wild-type mice, serum levels of IL-6 were one third lower in AAV-NT mice (Fig. 1C). While levels of STAT3 transcript and total protein were not statistically different between AAV-NT and wild-type livers, levels of the active p-STAT3-Y705 were markedly decreased in AAV-NT livers compared to controls (Fig. 1D). This correlated with a decreased nuclear translocated STAT3 protein in AAV-NT livers (Fig. 1E).

SIRT1 inactivates NFκB via deacetylation the K310 residue of the p65 subunit of NFκB (20,21). While hepatic levels of NFκB-p65 transcript and total protein were similar between AAV-NT and control mice (Fig. 2A), hepatic levels of the active protein, ac-NFκB-p65-K310 were lower in AAV-NT mice, compared to control mice (Fig. 2A). The sustained activation of STAT3/NFκB signaling promotes chronic inflammation and tumorigenesis through upregulation of genes involved in anti-apoptosis, proliferation and angiogenesis, many of which are interconnected (17). The down-regulation of hepatic STAT3/NFκB signaling in AAV-NT mice were evidenced by reduced hepatic levels of mRNAs and proteins for STAT3/NFκB targets, NOS2 (17,30), survivin (17,31) and MCP-1 (17), compared to controls (Fig. 2B and C). The chemokine MCP-1 promotes the accumulation of inflammatory macrophages (32). Immunofluorescence analysis showed that the numbers of hepatic macrophages were significantly lower in AAV-NT mice compared to the controls (Fig. 2D). The inflammatory HCAs are also characterized by high expression of C-reactive protein (CRP) and serum amyloid A2 (SAA2) (6,7). Compared to wild-type mice, hepatic mRNA levels for *Crp* and *Saa2* were significantly decreased in the AAV-NT mice along with decreased serum CRP protein levels (Fig. 2E). Collectively, the results suggest that downregulation of the inflammatory and tumorigenic pathways in the AAV-NT livers prevent HCA/HCC formation.

Activation of hepatic SIRT1/E-cadherin and FGF21/β-klotho signaling in AAV-NT mice

SIRT1 can function as a negative regulator of EMT in cancer metastasis by increasing the expression of E-cadherin and reducing the expression of mesenchymal marker proteins (23). Compared to wild-type mice, hepatic levels of mRNA (Fig. 3A) and protein (Fig. 3B) for E-cadherin were markedly increased in AAV-NT mice. Conversely, the AAV-NT livers showed decreased levels of mRNA and protein for the mesenchymal markers, N-cadherin, vimentin, and the EMT-inducing transcription factor, Slug, along with decreased mRNA levels for *Snail* (33), compared to wild-type livers (Fig. 3A and B).

The absence of HCA/HCC in AAV-NT mice suggests that additional CR responsive genes, including FGF21 (25,26) and its

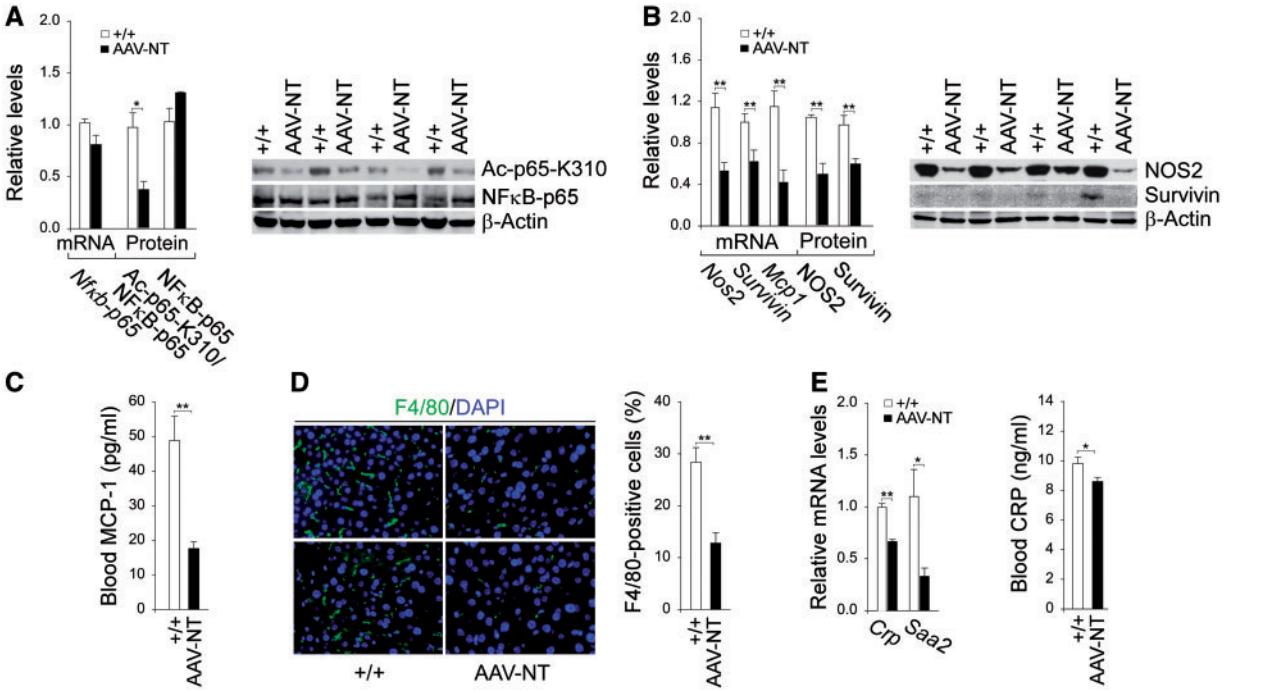

Figure 2. Analysis of hepatic NFκB signaling and inflammatory markers in 66–88 week-old wild-type and AAV-NT mice. For quantitative RT-PCR, the data were analyzed for wild-type (+/+, $n = 13$) and AAV-NT ($n = 22$) mice. For densitometry analysis, the data were analyzed from 4 pairs of wild-type/AAV-NT mice. The AAV-NT analyzed included AAV/3–63% ($n = 2$) and AAV/0.9–2.4%-NT ($n = 2$) mice. For blood MCP-1 and CRP levels, the data were analyzed for wild-type (+/+, $n = 12$) and AAV-NT ($n = 22$) mice. **(A)** Quantification *Nfκb-p65* mRNA by real-time RT-PCR; Western blot analysis of NFκB-p65, Ac-NFκB-p65-K310 and β-actin with quantification of protein levels by densitometry. **(B)** Quantification of mRNA for STAT3/NFκB targets by real-time RT-PCR; Western-blot analysis of NOS2, survivin and β-actin with quantification of protein levels by densitometry. **(C)** Blood MCP-1 levels. **(D)** Immunofluorescence analysis of hepatic cells stained positive for F4/80 that detects macrophages and quantification of F4/80-positive cells. Representative plates shown are analyzed for wild-type ($n = 6$) and AAV-NT ($n = 5$) mice. Scale bar: 25 μm. **(E)** Quantification of *Crp* and *Saa2* mRNA by real-time RT-PCR and blood CRP levels. Data represent the mean ± SEM; $^{*}P < 0.05$; $^{**}P < 0.005$.

co-receptor, the tumor suppressor β-klotho (25,28) may be induced. Indeed, levels of hepatic mRNA and protein for FGF21 and β-klotho were elevated in AAV-NT mice, compared to controls (Fig. 3C). β-Klotho suppresses hepatic expression of cholesterol 7a-hydroxylase (CYP7A1), the rate-limiting enzyme in hepatic bile acid synthesis (34). Consistent with this, levels of mRNA and protein for CYP7A1 were decreased in AAV-NT livers (Fig. 3C).

The frequency of β-catenin mutated HCA (28%) in GSD-I-associated HCA is significantly higher than the 7–14% found in non-GSD-associated β-catenin mutated HCA (6,7). The β-catenin protein is a key component of Wnt-canonical signaling pathway that is activated in many cancers, including HCC (35,36). The GSD-I-associated β-catenin mutated HCAs are characterized by high expression of two β-catenin targets glutamate-ammonia ligase (GLUL) and leucine-rich repeat containing G protein-coupled receptor 5 (LGR5) (6). While mRNA levels for *Lgr5* were markedly decreased in AAV-NT livers, levels of mRNA and protein for β-catenin and GLUL were unchanged, compared to control livers (Fig. 3D). Following translocation into the nucleus, β-catenin binds to the TCF/LEF (T-cell factor/lymphoid enhancer factor) and activates the expression of target genes (35,36). LEF-1 is also a β-catenin target (35). In AAV-NT livers, *Lef1* mRNA levels were significantly decreased, compared to controls (Fig. 3D).

A SIRT1 inhibitor reverses the tumor antagonizing environment in AAV-NT livers

The activation of AMPK/SIRT1/FGF21/β-klotho and down-regulation of STAT3/NFκB signaling pathways suggest that the livers of AAV-NT mice exhibiting a tumor antagonizing environment. FGF21 is a downstream target of SIRT1 (27) and SIRT1 can regulate AMPK via deacetylation and activation of liver kinase B1 (LKB1) (13,37), a primary AMPK kinase that phosphorylates and activates AMPK (38). To demonstrate that signaling by SIRT1 plays a major role influencing the environment for tumor formation, we treated 64–74 week-old wild-type and AAV-NT mice with 6-chloro-2,3,4,9-tetrahydro-1H-carbazole-1-carboxamide (EX-527), a potent, selective, NAD^{+}-dependent SIRT1 inhibitor (39). We then examined their phenotype after 4 consecutive weeks of exposure. EX-527 treatment did not alter body weight and body fat values of both wild-type and AAV-NT mice (Fig. 4A). Also, EX-527-treated wild-type and AAV-NT mice could tolerate long fasts and their 24 hour fasted glucose levels were comparable to the levels prior to EX-527 treatment (Fig. 4A).

Compared to wild-type mice, hepatic protein levels of AMPK were elevated in AAV-NT mice both before and after EX-527 treatment (Fig. 4B). However, the increase in p-AMPK-T172 was significantly reduced by EX-527 (Fig. 4B), suggesting that SIRT1 may regulate AMPK via LKB1 (13,37,38). Importantly, the liver phenotype of reduced inflammation seen in AAV-NT mice was reversed following EX-527 treatment. In wild-type mice, hepatic levels of active, pro-inflammatory p-STAT3-Y705 and ac-NFκB-p65-K310 remained similar before and after EX-527 treatment (Fig. 4C). In contrast, in AAV-NT mice, hepatic levels of both p-STAT3-Y705 and ac-NFκB-p65-K310 proteins were markedly increased after EX-527 treatment (Fig. 4C), indicating the reversal of anti-inflammation. This phenotypic change also suggested that the expression of STAT3/NFκB target genes should

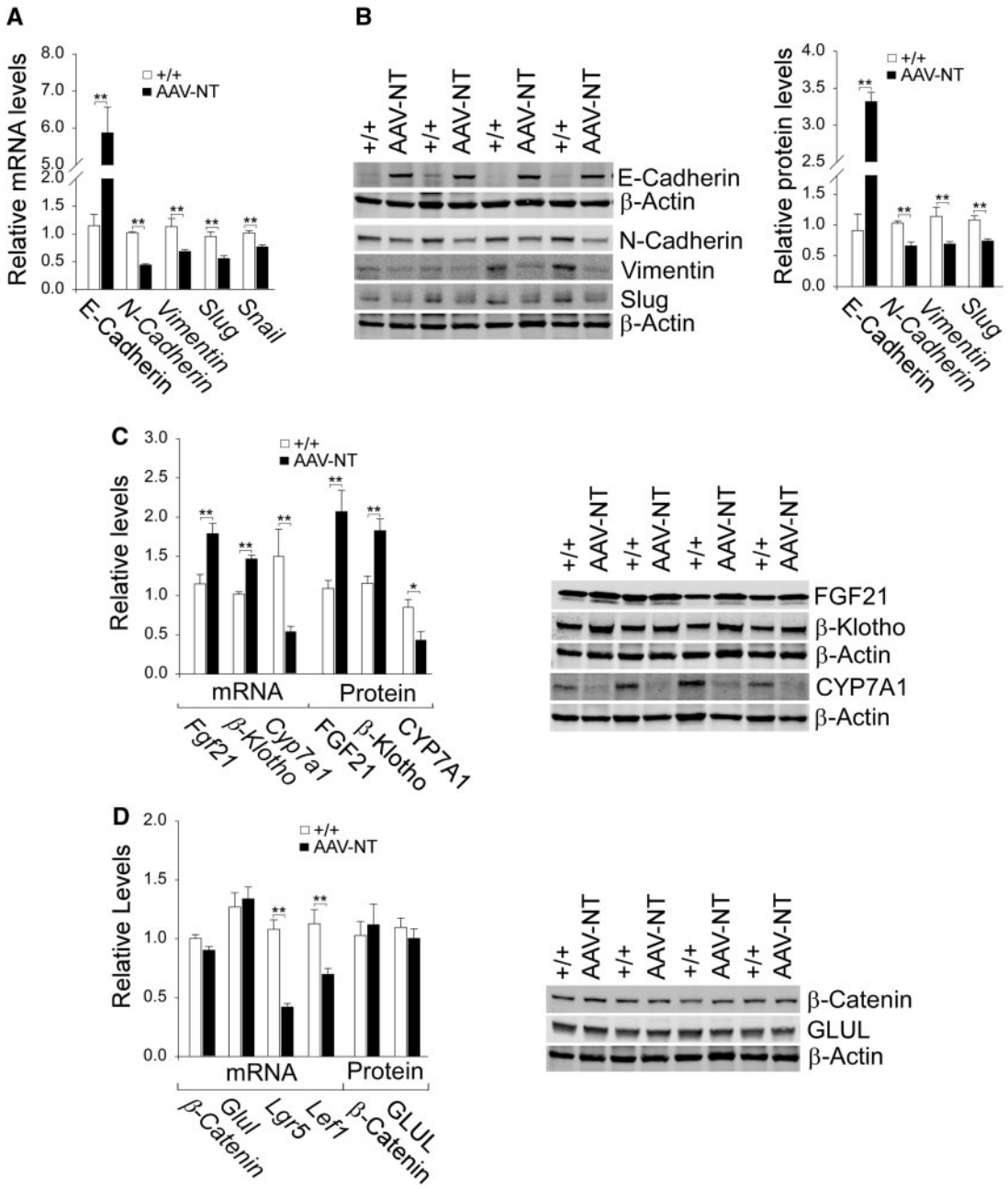

Figure 3. Analysis of hepatic E-cadherin, mesenchymal markers, FGF21, β-klotho and β-catenin targets in 66–88 week-old wild-type and AAV-NT mice. For quantitative RT-PCR, the data were analyzed for wild-type (+/+, $n = 13$) and AAV-NT ($n = 22$) mice. For densitometry analysis, the data were analyzed from 4 pairs of wild-type/AAV-NT mice. The AAV-NT analyzed included AAV/3-63% ($n = 2$) and AAV/0.9–2.4%-NT ($n = 2$) mice. **(A)** Quantification of *E-cadherin*, *N-cadherin*, *vimentin*, *Slug* and *Snail* mRNA by real-time RT-PCR. **(B)** Western blot analysis of E-cadherin, N-cadherin, vimentin, Slug and β-actin with quantification of protein levels by densitometry. **(C)** Quantification *β-Klotho*, *Fgf21* and *Cyp7a1* mRNA by real-time RT-PCR; Western blot analysis of FGF21, β-klotho, CYP7A1 and β-actin; and quantification of protein levels by densitometry. **(D)** Quantification of *β-Catenin*, *Glul*, *Lgr5*, *Cyclin D1* and *Lef1* mRNA by real-time RT-PCR; Western-blot analysis of β-catenin, GLUL and β-actin; and quantification protein levels by densitometry. Data represent the mean ± SEM; $^{*}P < 0.05$; $^{**}P < 0.005$.

also be altered. Indeed, while hepatic protein levels of NOS2 (17,30) and survivin (17,31) in wild-type mice remained statistically similar before and after EX-527 treatment (Fig. 5A), hepatic protein levels of both NOS2 and survivin in AAV-NT mice were markedly increased after EX-527 treatment (Fig. 5A). Immunofluorescence analysis further showed that the numbers of hepatic macrophages in wild-type mice remained similar before and after EX-527 treatment but the numbers of hepatic macrophages in AAV-NT mice were increased greatly after EX-527 treatment (Fig. 5B). Taken together, the results suggest that the SIRT1 pathway is activated in the livers of the AAV-NT mice and that inhibition of SIRT1 signaling by EX-527 can reverse many of anti-inflammatory/anti-tumorigenic changes mediated by SIRT1.

EX-527 treatment also selectively reduced the increase in hepatic levels of E-cadherin in AAV-NT mice (Fig. 6A). Moreover, EX-527 selectively increased hepatic levels of N-cadherin and the EMT-inducing transcription factor Slug in AAV-NT mice

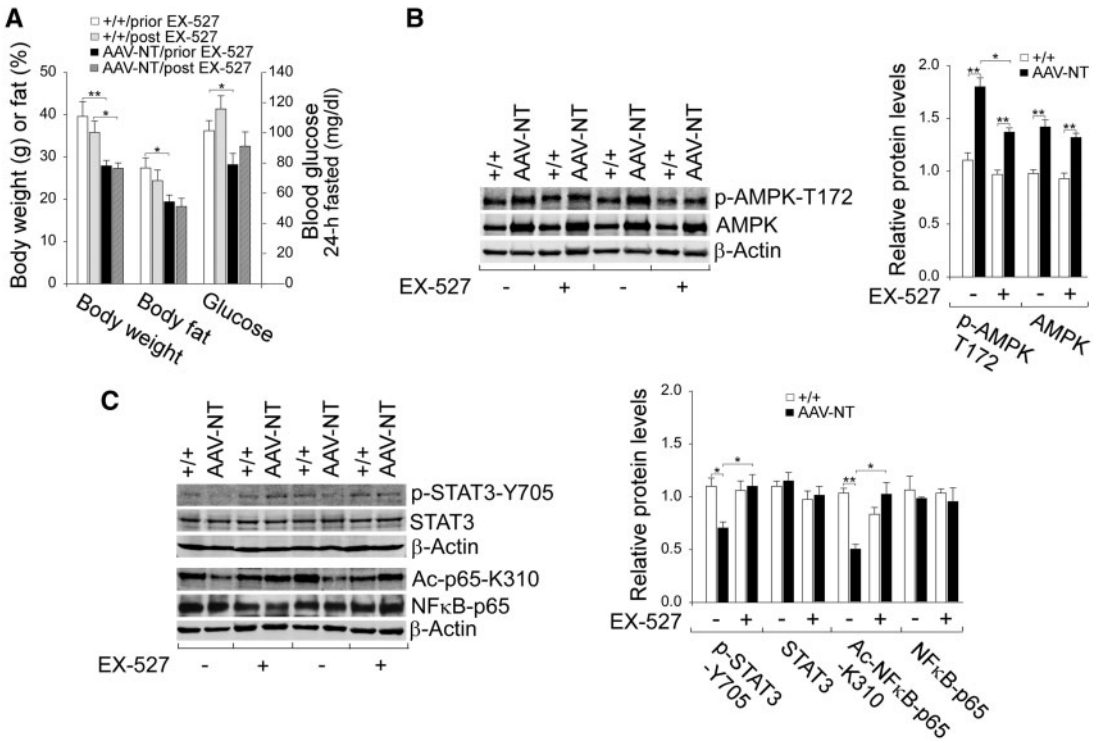

Figure 4. Effects of EX-527 on AMPK/STAT3/NFκB signaling in wild-type and AAV-NT mice. Wild-type and AAV-NT mice at age 64–74 weeks were treated daily for four weeks with EX-527 and their phenotype analyzed at age 68–78 weeks. For quantitative RT-PCR, the data were analyzed for wild-type (+/+, $n=8$), wild-type-EX-527 (+/+/EX-527, $n=8$), AAV-NT ($n=8$) and AAV-NT-EX-527 ($n=8$) mice. For densitometry analysis, the data were analyzed from 4 pairs of wild-type/AAV-NT and wild-type-EX-527/AAV-NT-EX-527 mice. **(A)** Body weight, body fat and fasting blood glucose levels of mice before and after EX-527 treatment. **(B)** Western blot analysis of p-AMPK-T172, AMPK and β-actin with quantification of protein levels by densitometry. **(C)** Western-blot analysis of p-STAT3-Y705, STAT3, NFκB-p65, Ac-NFκB-p65-K310 and β-actin and quantification protein levels by densitometry. Data represent the mean ± SEM; $^{*}P<0.05$; $^{**}P<0.005$.

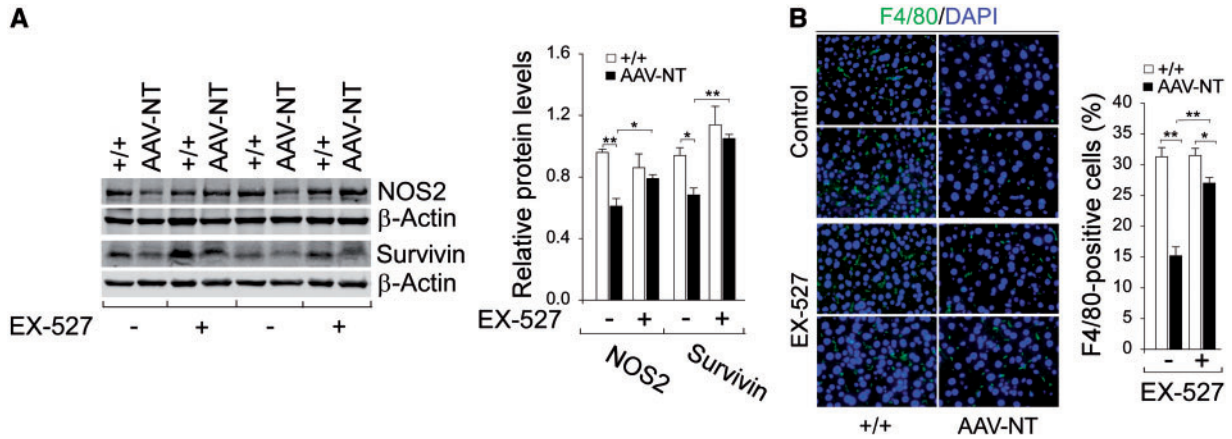

Figure 5. Effects of EX-527 on hepatic STAT3/NFκB targets in wild-type and AAV-NT mice. Wild-type and AAV-NT mice at age 64–74 weeks were treated with EX-527 for 4 weeks, and their phenotype analyzed at age 68–78 weeks. For densitometry analysis, the data were analyzed from 4 pairs of wild-type/AAV-NT and wild-type-EX-527/AAV-NT-EX-527 mice. **(A)** Western blot analysis of NOS2, survivin, and β-actin with quantification of protein levels by densitometry. **(B)** Immunofluorescence analysis of hepatic cells stained positive for F4/80 that detects macrophages and quantification of F4/80-positive cells. Representative plates shown are analyzed for 4 pairs of wild-type/AAV-NT and wild-type-EX-527/AAV-NT-EX-527 mice. Scale bar: 25 μm. Data represent the mean ± SEM; $^{*}P<0.05$; $^{**}P<0.005$.

(Fig. 6A). Prior to EX-527 treatment, hepatic levels of vimentin were marked lower in AAV-NT mice compared to wild-type mice (Fig. 6A). After EX-527 treatment, hepatic levels of vimentin became similar between wild-type and AAV-NT mice (Fig. 6A). Taken together, the results again suggest that EX-527 can reverse the SIRT1-mediated anti-metastatic liver phenotype of the AAV-NT mice.

Prior to EX-527 treatment, hepatic levels of FGF21 were significantly higher in AAV-NT mice, compared to control mice (Fig. 6B). After EX-527 treatment, while hepatic levels of FGF21 remained unchanged in wild-type mice, hepatic levels of FGF21 were markedly decreased in AAV-NT mice (Fig. 6B). Both FGF21 and its co-receptor β-klotho are CR responsive genes (25) but only FGF21 has been shown to be a target gene of SIRT1 (27).

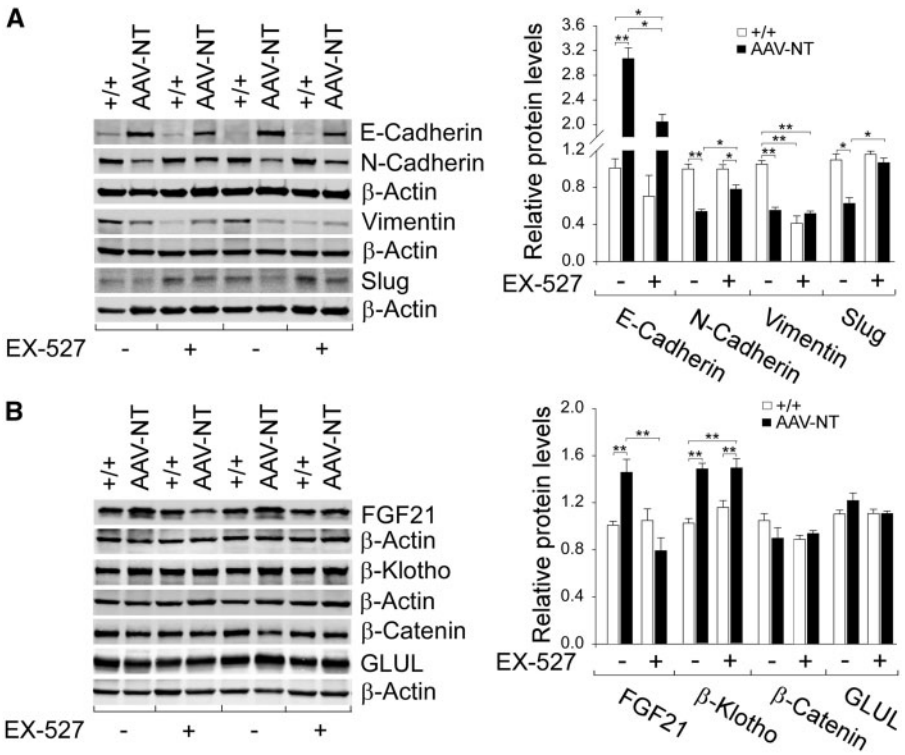

Figure 6. Effects of EX-527 on hepatic E-cadherin, mesenchymal markers, FGF21 and β-klotho in wild-type and AAV-NT mice. Wild-type and AAV-NT mice at age 64–74 weeks were treated with EX-527 for 4 weeks, and their phenotype analyzed at age 68–78 weeks. For densitometry analysis, the data were analyzed from 4 pairs of wild-type/AAV-NT and wild-type-EX-527/AAV-NT-EX-527 mice. **(A)** Western blot analysis of E-cadherin, N-cadherin, vimentin, slug and β-actin with quantification of protein levels by densitometry. **(B)** Western-blot analysis of FGF21, β-klotho, β-catenin, GLUL and β-actin and quantification protein levels by densitometry. Data represent the mean ± SEM; $^{*}P < 0.05$; $^{**}P < 0.005$.

Indeed, hepatic levels of β-klotho remained similar in control and AAV-NT mice before and after EX-527 treatment (Fig. 6B), suggesting CR-mediated β-klotho activation is independent of SIRT1 action. Also, hepatic protein levels of β-catenin, activated in many cancers (35,36) and GLUL, activated in GSD-I-associated β-catenin mutated HCAs and a β-catenin targets (6,7) were also unchanged following EX-527 treatment (Fig. 6B).

Discussion

GSD-Ia is juvenile lethal unless the loss of blood glucose homeostasis is addressed (1,2). While dietary therapies (3,4) have enabled GSD-Ia patients under strict compliance to maintain normoglycemia, the therapies do not address the serious long-term complications of HCA/HCC with unknown etiology (1,2). Using rAAV-mediated gene therapy, we have previously shown that the rAAV-treated mice reconstituted with 3–63% (5–108 units) of normal hepatic G6Pase-α activity (averaged 171.4 ± 5.7 units) maintain blood glucose homeostasis and do not develop HCA/HCC (8,9). We further showed that 75% of the *G6pc*-/- mice reconstituted with 0.9–2.4% (1.5–4.1 units) of normal hepatic G6Pase-α activity exhibited a similar phenotype (10). Moreover, the non-tumor-bearing AAV-NT mice reconstituted with 0.9–63% of normal hepatic G6Pase-α activity are protected against age-related insulin resistance and obesity, and exhibit a phenotype mimicking animals living under CR (8–10). In this study, we provide evidence showing that the absence of HCA/HCC in AAV-NT mice is correlated with up-regulation of hepatic AMPK/SIRT1and FGF21/β-klotho signaling and down-regulation of STAT3/NFκB-mediated inflammatory and tumorigenic signaling pathways (Fig. 7).

The available evidence indicates that activation of signaling pathways of the two CR modulators AMPK (14,15) and SIRT1 (18,19) underlies, at least in part, the absence of HCA/HCC in AAV-NT mice. Firstly, studies have shown that chronic inflammation triggers cellular events that promote malignant transformation of cells through the sustained activation of the signaling pathways of two pro-inflammatory transcription factors–STAT3 and NFκB (17,22). AMPK inhibits the IL-6-mediated phosphorylation and activation of STAT3 (16), while SIRT1-mediated deacetylation of NFκB-p65 inhibits NFκB activity (20,21). STAT3 interacts with NFκB at multiple levels and together they regulate numerous genes important for cancer-promoting inflammation (17,22). In non-tumor-bearing AAV-NT mice, the simultaneous inhibition of hepatic STAT3 and NFκB signaling results in: decreased expression of their targets NOS2 and survivin; reduced serum levels of MCP-1 and IL-6; and reduced accumulation of inflammatory macrophages. Secondly, SIRT1 negatively regulates tumor metastasis by increasing the expression of E-cadherin and inhibiting the expression of mesenchymal markers (23,24). In AAV-NT livers, hepatic expression of the tumor suppressor E-cadherin was increased along with decreased hepatic expression of mesenchymal markers, N-cadherin and vimentin and decreased hepatic expression of EMT-inducing transcription factors, Slug and Snail. Thirdly, the reduced inflammatory and tumorigenic pathway signaling observed in the liver of AAV-NT mice was reversed by treating 64–74 week-old wild-type and AAV-NT mice with a potent, NAD^{+}-dependent SIRT1 inhibitor, EX-527 (39). Studies have shown that AMPK and SIRT1 regulate each other (13) and SIRT1 can activate AMPK via

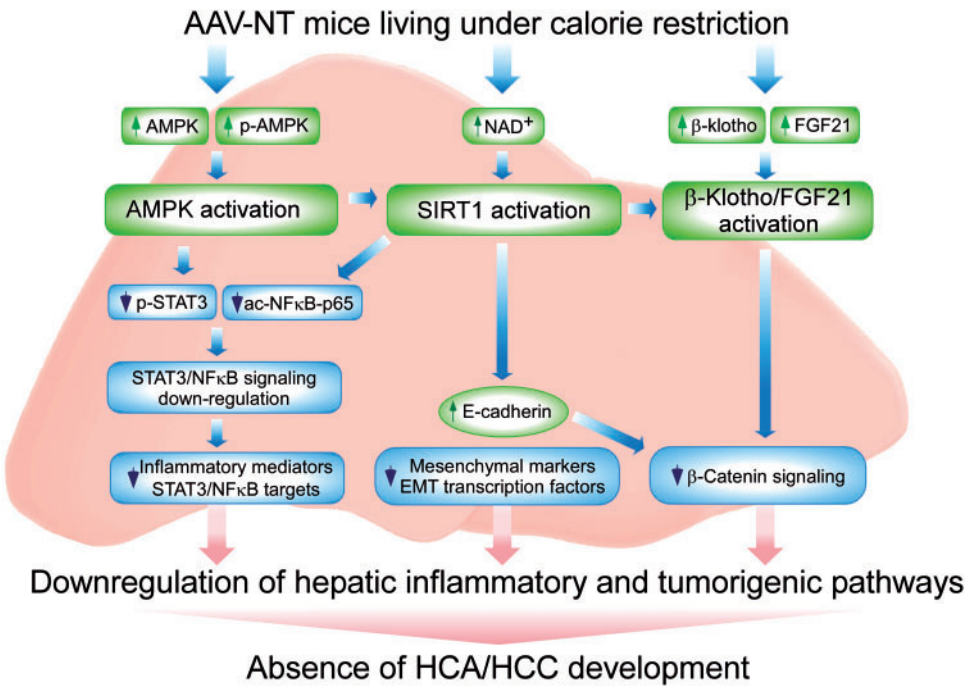

Figure 7. Hepatic signaling pathways underlying the absence of HCA/HCC in *G6pc*-/- mice receiving gene therapy and living under calorie restriction. Several signaling pathways implicated in inflammation and tumorigenesis are downregulated in the liver of AAV-NT mice, contributing to the absence of hepatic tumors. The increases in total AMPK and p-AMPK-T172 activate AMPK that suppresses phosphorylation and activation of STAT3 signaling. The increase in hepatic NAD^+ levels activates SIRT1 that suppresses NFκB signaling via deacetylation of the p65 subunit of NFκB. The down-regulation of hepatic STAT3/NFκB signaling leads to reduced expression of inflammatory and tumorigenic STAT3/NFκB targets. SIRT1 activation also negatively regulates tumor metastasis by increasing the expression of E-cadherin and reducing the expression of mesenchymal markers and the EMT transcription factors. The increase in E-cadherin also inhibits β-catenin signaling that plays a key role in the pathogenesis of HCC. CR also activates FGF21/β-klotho signaling that decreases the expression of β-catenin targets and prevents hepatocarcinogenesis.

deacetylation and activation of LKB1 (37), a major AMPK kinase that phosphorylates and activates AMPK at T172 (38). Indeed, EX-527 treatment selectively reduced hepatic levels of the activated p-AMPK-T172 in AAV-NT mice. Accordingly, hepatic levels of the activated p-STAT3-Y705 and ac-NFκB-p65-K310 were markedly increased in EX-527 treated AAV-NT mice, compared to untreated AAV-NT mice. The activation of hepatic STAT3 and NFκB signaling in EX-527-treated AAV-NT mice results in increased hepatic expression of NOS2, survivin and increased hepatic accumulation of inflammatory macrophages, compared to untreated AAV-NT mice. Moreover, in EX-527-treated AAV-NT mice, hepatic expression of the tumor suppressor E-cadherin was decreased along with increased hepatic expression of N-cadherin and Slug. Also, while hepatic vimentin levels in AAV-NT mice were significantly lower than that in wild-type mice prior to EX-527 treatment, hepatic vimentin levels in AAV-NT mice became similar to wild-type mice after EX-527 treatment. Taken together our results indicate that downregulation of the inflammatory and tumorigenic signaling pathways in the liver of AAV-NT mice were reversed via inhibition of SIRT1 activity by EX-527.

Studies have shown that CR increases the expression of FGF21 (25), a downstream target of SIRT1 (27) as well as β-klotho (25), a tumor suppressor and a FGF21 co-receptor (26,28). FGF21 plays a major role in stimulating energy expenditure and improving insulin sensitivity (26). A recent study also showed that FGF21 can prevent chemical-induced hepatocarcinogenesis by upregulating the expression of β-klotho (29). In AAV-NT mice, hepatic expression of both FGF21 and β-klotho was upregulated. The frequency of β-catenin-activated HCA (28%) in GSD-I-associated HCA is significantly higher than the 7–14% found in non-GSD-associated β-catenin mutated HCA (6,7). Although a direct link between β-klotho and β-catenin signaling has not been established, β-klotho was shown to inhibit the expression of cyclin D1, a β-catenin target, (28), suggesting that β-klotho might repress β-catenin signaling. β-Catenin is a major effector of the Wnt/β-catenin signaling that plays a key role in the pathogenesis of HCC (35,36). Activation of Wnt signaling leads to accumulation and nuclear translocation of β-catenin, and in the nucleus, β-catenin interacts with TCF/LEF regulating the expression of target genes (35,36). Moreover, E-cadherin can impede β-catenin signaling via interaction with the catenins forming the cadherin-catenin complex (24). In AAV-NT mice, hepatic expression of β-catenin targets, *Lef1* and *Lgr5*, was reduced. Collectively, activation of FGF21/β-klotho signaling pathway provides another mechanism underlying the absence of HCA/HCC in AAV-NT livers.

In summary, we showed that the underlying mechanisms responsible for the absence of HCA/HCC in AAV-NT mice correlate with activation of hepatic AMPK/SIRT1 and β-klotho/FGF21 signaling and down-regulation of STAT3 and NFκB signaling pathways. The finding that a moderate reduction of hepatic G6Pase-α activity in mice generates a liver environment with reduced inflammatory and tumorigenic responses provides insight into the biology and pathogenesis of the role of G6Pase-α in hepatic tumorigenesis.

Materials and Methods

The rAAV-infused *G6pc*-/- mice

All animal studies were conducted under an animal protocol approved by the Eunice Kennedy Shriver National Institute of

Child Health and Human Development Animal Care and Use Committee. The *G6pc*-/- mice infused with either AAV-G6PC or AAV-co-G6PC and the age-matched *G6pc*+/+ and *G6pc*+/- mice with indistinguishable phenotype (referred collectively as wild-type or control mice) have been described (10). Liver samples were collected from wile-type and AAV-NT mice at sacrifice following a 24-hour fast to ensure that hepatic glucose is produced mainly via gluconeogenesis (10).

Wild-type and AAV-NT mice at age 64–74 weeks were injected intraperitoneally with EX-527 (39) (Sigma-Aldrich, St. Louis, MO, USA) at 2 mg/kg daily for 4 weeks (40). Liver samples were collected at sacrifice following a 24-hour fast at age 68–78 weeks.

Phenotype analysis. Body composition was assessed using the Bruker minispec NMR analyzer (Karlsruhe, Germany). Blood levels of glucose and hepatic levels of NAD^+ were determined as described previously (8,9). Blood levels of CRP, MCP-1, and IL-6 were determined using the C Reactive Protein Mouse ELISA Kit (Abcam, Cambridge, MA, USA), Mouse/Rat MCP-1 Quantikine ELISA Kit and Mouse IL-6 Quantikine ELISA Kit (R&D Systems Inc., Minneapolis, MN, USA), respectively.

Quantitative real-time RT-PCR and western-blot analysis. The mRNA expression was quantified by real-time RT-PCR using the TaqMan probes in an Applied Biosystems QuantStudio 3 Real-Time PCR System (Foster City, CA, USA). Data were normalized to Rpl19 RNA. Western-blot images were detected using the LI-COR Odyssey scanner and the Image studio 3.1 software (Li-Cor Biosciences, Lincoln, NE, USA). Mouse monoclonal antibodies used from Santa Cruz Biotechnology (Dallas, TX, USA) were β-actin; from Cell Signaling (Danvers, MA, USA) were: E-cadherin, N-cadherin, STAT3 and NFκB-p65. Rabbit monoclonal antibodies used from Cell Signaling were: β-catenin, Slug, vimentin, p-STAT3-Y705, survivin, NOS2; and from Abcam were: FGF21, p-AMPK-T172, NFκB-p65-K310. Rabbit polyclonal antibodies used were ChREBP (Novus biologicals, Littleton, CO, USA); AMPK (Cell Signaling); GLUL (Abcam); SIRT1 (Milipore, Billerica, MA, USA) and CYP7A1 (Santa Cruz Biotechnology). Goat polyclonal antibody used was β-klotho (Santa Cruz Biotechnology). Protein expression was quantified by densitometry using the Multi-Gauge version 3.0 software (Fujifilm, Japan).

Immunofluorescence analysis. Mouse liver paraffin sections (10 μm thickness) were treated with ImmunoDNA Retriever EDTA buffer (Bio SB, Inc. Goleta, CA, USA) and blocked with PBS containing 10% fetal bovine serum and 5% bovine serum albumin. For STAT3 detection, the liver sections were incubated with a mouse monoclonal antibody against STAT3 (Cell Signaling) and for macrophage detection, the liver sections were incubated with a rat monoclonal antibody against F4/80 (Abcam). The liver sections were then incubated with the appropriate IgG antibody, conjugated with Alexa Fluor 488 or 555 (Invitrogen, Carlsbad, CA, USA), mounted with an anti-fade medium containing DAPI (Vector Laboratories, Burlingame, CA, USA) and visualized using a Zeiss Axioskop2 plus microscope (Carl Zeiss MicroImaging, Germany). Images were acquired using a Nikon DS-Fil digital camera and NIS-Elements F3.0 imaging software (Nikon, Japan).

Statistical analysis. The unpaired *t*-test was performed using the GraphPad Prism Program, version 4 (San Diego, CA, USA). Values were considered statistically significant at $P < 0.05$.

Conflict of Interest statement. None declared.

Funding

This research was supported by the Intramural Research Program of the Eunice Kennedy Shriver National Institute of Child Health and Human Development, National Institutes of Health, and The Children's Fund for Glycogen Storage Disease Research.

References

1. Chou, J.Y., Jun, H.S. and Mansfield, B.C. (2010) Glycogen storage disease type I and G6Pase-β deficiency: etiology and therapy. *Nat. Rev. Endocrinol.*, **6**, 676–688.
2. Rake, J.P., Visser, G., Labrune, P., Leonard, J.V., Ullrich, K. and Smit, G.P. (2002) Glycogen storage disease type I: diagnosis, management, clinical course and outcome. Results of the European Study on Glycogen Storage Disease Type I (ESGSD I). *Eur. J. Pediatr.*, **161 (Suppl 1)**, S20–S34.
3. Greene, H.L., Slonim, A.E., O'Neill, J.A., Jr and Burr, I.M. (1976) Continuous nocturnal intragastric feeding for management of type 1 glycogen-storage disease. *N. Engl. J. Med.*, **294**, 423–425.
4. Chen, Y.T., Cornblath, M. and Sidbury, J.B. (1984) Cornstarch therapy in type I glycogen-storage disease. *N. Engl. J. Med.*, **310**, 171–175.
5. Franco, L.M., Krishnamurthy, V., Bali, D., Weinstein, D.A., Arn, P., Clary, B., Boney, A., Sullivan, J., Frush, D.P., Chen, Y.T. *et al.* (2005) Hepatocellular carcinoma in glycogen storage disease type Ia: a case series. *J. Inherit. Metab. Dis.*, **28**, 153–162.
6. Calderaro, J., Labrune, P., Morcrette, G., Rebouissou, S., Franco, D., Prevot, S., Quaglia, A., Bedossa, P., Libbrecht, L., Terracciano, L. *et al.* (2013) Molecular characterization of hepatocellular adenomas developed in patients with glycogen storage disease type I. *J. Hepatol.*, **58**, 350–357.
7. Pilati, C. and Zucman-Rossi, J. (2015) Mutations leading to constitutive active gp130/JAK1/STAT3 pathway. *Cytokine Growth Factor Rev.*, **26**, 499–506.
8. Lee, Y.M., Jun, H.S., Pan, C.J., Lin, S.R., Wilson, L.H., Mansfield, B.C. and Chou, J.Y. (2012) Prevention of hepatocellular adenoma and correction of metabolic abnormalities in murine glycogen storage disease type Ia by gene therapy. *Hepatology*, **56**, 1719–1729.
9. Kim, G.Y., Lee, Y.M., Cho, J.H., Pan, C.J., Jun, H.S., Springer, D.A., Mansfield, B.C. and Chou, J.Y. (2015) Mice expressing reduced levels of hepatic glucose-6-phosphatase-alpha activity do not develop age-related insulin resistance or obesity. *Hum. Mol. Genet.*, **24**, 5115–5125.
10. Kim, G.Y., Lee, Y.M., Kwon, J.H., Cho, J.H., Mansfield, B.C. and Chou, J.Y. (2017) Glycogen storage disease type Ia mice with less than 2% of normal hepatic glucose-6-phosphatase-α activity restored are at risk of developing hepatic tumors. *Mol. Genet. Metab.*, **120**, 229–324.
11. Lee, Y.M., Kim, G.Y., Pan, C.J., Mansfield, B.C. and Chou, J.Y. (2015) Minimal hepatic glucose-6-phosphatase-alpha activity required to sustain survival and prevent hepatocellular adenoma formation in murine glycogen storage disease type Ia. *Mol. Genet. Metab. Rep.*, **3**, 28–32.
12. Lee, Y.M., Pan, C.J., Koeberl, D.D., Mansfield, B.C. and Chou, J.Y. (2013) The Upstream enhancer elements of the *G6PC* promoter are critical for optimal G6PC expression in murine glycogen storage disease type Ia. *Mol. Genet. Metab.*, **110**, 275–280.

13. Ruderman, N.B., Xu, X.J., Nelson, L., Cacicedo, J.M., Saha, A.K., Lan, F. and Ido, Y. (2010) AMPK and SIRT1: a long-standing partnership? *Am. J. Physiol. Endocrinol. Metab.*, **298**, E751–E760.
14. Cantó, C. and Auwerx, J. (2011) Calorie restriction: is AMPK a key sensor and effector? *Physiol. (Bethesda)*, **26**, 214–224.
15. Hardie, D.G. (2011) AMP-activated protein kinase: an energy sensor that regulates all aspects of cell function. *Genes Dev.*, **25**, 1895–1908.
16. Nerstedt, A., Cansby, E., Amrutkar, M., Smith, U. and Mahlapuu, M. (2013) Pharmacological activation of AMPK suppresses inflammatory response evoked by IL-6 signalling in mouse liver and in human hepatocytes. *Mol. Cell Endocrinol.*, **375**, 68–78.
17. Yu, H., Pardoll, D. and Jove, R. (2009) STATs in cancer inflammation and immunity: a leading role for STAT3. *Nat. Rev. Cancer*, **9**, 798–809.
18. Mouchiroud, L., Houtkooper, R.H. and Auwerx, J. (2013) NAD(+) metabolism: a therapeutic target for age-related metabolic disease. *Crit. Rev. Biochem. Mol. Biol.*, **48**, 397–408.
19. Poulose, N. and Raju, R. (2015) Sirtuin regulation in aging and injury. *Biochim. Biophys. Acta*, **1852**, 2442–2455.
20. Yeung, F., Hoberg, J.E., Ramsey, C.S., Keller, M.D., Jones, D.R., Frye, R.A. and Mayo, M.W. (2004) Modulation of NF-kappaB-dependent transcription and cell survival by the SIRT1 deacetylase. *EMBO J.*, **23**, 2369–2380.
21. Lu, J., Zhang, L., Chen, X., Lu, Q., Yang, Y., Liu, J. and Ma, X. (2014) SIRT1 counteracted the activation of STAT3 and NF-kappaB to repress the gastric cancer growth. *Int. J. Clin. Exp. Med.*, **7**, 5050–5058.
22. He, G. and Karin, M. (2011) NF-κB and STAT3–key players in liver inflammation and cancer. *Cell Res.*, **21**, 159–168.
23. Chen, I.C., Chiang, W.F., Huang, H.H., Chen, P.F., Shen, Y.Y. and Chiang, H.C. (2014) Role of SIRT1 in regulation of epithelial-to-mesenchymal transition in oral squamous cell carcinoma metastasis. *Mol. Cancer*, **13**, 254.
24. Liu, X. and Chu, K.M. (2014) E-cadherin and gastric cancer: cause, consequence, and applications. *Biomed. Res. Int.*, **2014**, 637308.
25. Fletcher, J.A., Meers, G.M., Laughlin, M.H., Ibdah, J.A., Thyfault, J.P. and Rector, R.S. (2012) Modulating fibroblast growth factor 21 in hyperphagic OLETF rats with daily exercise and caloric restriction. *Appl. Physiol. Nutr. Metab.*, **37**, 1054–1062.
26. Fisher, F.M. and Maratos-Flier, E. (2016) Understanding the physiology of FGF21. *Annu. Rev. Physiol.*, **78**, 223–241.
27. Li, Y., Wong, K., Giles, A., Jiang, J., Lee, J.W., Adams, A.C., Kharitonenkov, A., Yang, Q., Gao, B., Guarente, L. *et al.* (2014) Hepatic SIRT1 attenuates hepatic steatosis and controls energy balance in mice by inducing fibroblast growth factor 21. *Gastroenterology*, **146**, 539–549. e537.
28. Ye, X., Guo, Y., Zhang, Q., Chen, W., Hua, X., Liu, W., Yang, Y. and Chen, G. (2013) betaKlotho suppresses tumor growth in hepatocellular carcinoma by regulating Akt/GSK-3beta/cyclin D1 signaling pathway. *PLoS One*, **8**, e55615.
29. Xu, P., Zhang, Y., Wang, W., Yuan, Q., Liu, Z., Rasoul, L.M., Wu, Q., Liu, M., Ye, X., Li, D. *et al.* (2015) Long-term administration of fibroblast growth factor 21 prevents chemically-induced hepatocarcinogenesis in mice. *Dig. Dis. Sci.*, **60**, 3032–3043.
30. Iwakiri, Y. and Kim, M.Y. (2015) Nitric oxide in liver diseases. *Trends. Pharmacol. Sci.*, **36**, 524–536.
31. Subramaniam, A., Shanmugam, M.K., Perumal, E., Li, F., Nachiyappan, A., Dai, X., Swamy, S.N., Ahn, K.S., Kumar, A.P., Tan, B.K. *et al.* (2013) Potential role of signal transducer and activator of transcription (STAT)3 signaling pathway in inflammation, survival, proliferation and invasion of hepatocellular carcinoma. *Biochim. Biophys. Acta*, **1835**, 46–60.
32. Zimmermann, H.W., Trautwein, C. and Tacke, F. (2012) Functional role of monocytes and macrophages for the inflammatory response in acute liver injury. *Front Physiol.*, **3**, 56.
33. Tania, M., Khan, M.A. and Fu, J. (2014) Epithelial to mesenchymal transition inducing transcription factors and metastatic cancer. *Tumour. Biol.*, **35**, 7335–7342.
34. Ito, S., Fujimori, T., Furuya, A., Satoh, J. and Nabeshima, Y. (2005) Impaired negative feedback suppression of bile acid synthesis in mice lacking betaKlotho. *J. Clin. Invest.*, **115**, 2202–2208.
35. Herbst, A., Jurinovic, V., Krebs, S., Thieme, S.E., Blum, H., Goke, B. and Kolligs, F.T. (2014) Comprehensive analysis of beta-catenin target genes in colorectal carcinoma cell lines with deregulated Wnt/beta-catenin signaling. *BMC Genom.*, **15**, 74.
36. Pez, F., Lopez, A., Kim, M., Wands, J.R., Caron de Fromentel, C. and Merle, P. (2013) Wnt signaling and hepatocarcinogenesis: molecular targets for the development of innovative anticancer drugs. *J. Hepatol.*, **59**, 1107–1117.
37. Lan, F., Cacicedo, J.M., Ruderman, N. and Ido, Y. (2008) SIRT1 modulation of the acetylation status, cytosolic localization, and activity of LKB1. Possible role in AMP-activated protein kinase activation. *J. Biol. Chem.*, **283**, 27628–27635.
38. Korsse, S.E., Peppelenbosch, M.P. and van Veelen, W. (2013) Targeting LKB1 signaling in cancer. *Biochim. Biophys. Acta*, **1835**, 194–210.
39. Gertz, M., Fischer, F., Nguyen, G.T., Lakshminarasimhan, M., Schutkowski, M., Weyand, M. and Steegborn, C. (2013) Ex-527 inhibits Sirtuins by exploiting their unique NAD^+-dependent deacetylation mechanism. *Proc. Natl. Acad. Sci. USA*, **110**, E2772–E2781.
40. Zhou, X., Fan, L.X., Sweeney, W.E., Jr, Denu, J.M., Avner, E.D. and Li, X. (2013) Sirtuin 1 inhibition delays cyst formation in autosomal-dominant polycystic kidney disease. *J. Clin. Invest.*, **123**, 3084–3098.